Purification and Characterization of the Epoxidase Catalyzing the Formation of Fosfomycin from *Pseudomonas syringae*[†]

Jeffrey W. Munos,[‡,§] Sung-Ju Moon,[‡,||] Steven O. Mansoorabadi,[‡] Weichen Chang,[‡] Lin Hong,[‡,⊥] Feng Yan,[‡,@] Aimin Liu,[▽] and Hung-wen Liu*[,‡]

Division of Medicinal Chemistry, College of Pharmacy, and Department of Chemistry and Biochemistry, University of Texas, Austin, Texas 78712, and Department of Chemistry, Georgia State University, Atlanta, Georgia 30302-4098

Received May 12, 2008; Revised Manuscript Received June 11, 2008

ABSTRACT: The final step in the biosynthesis of fosfomycin in *Streptomyces wedmorensis* is catalyzed by (*S*)-2-hydroxypropylphosphonic acid (HPP) epoxidase (*Sw*-HppE). A homologous enzyme from *Pseudomonas syringae* whose encoding gene (*orf3*) shares a relatively low degree of sequence homology with the corresponding *Sw*-HppE gene has recently been isolated. This purified *P. syringae* protein was determined to catalyze the epoxidation of (*S*)-HPP to fosfomycin and the oxidation of (*R*)-HPP to 2-oxopropylphosphonic acid under the same conditions as *Sw*-HppE. Therefore, this protein is indeed a true HPP epoxidase and is termed *Ps*-HppE. Like *Sw*-HppE, *Ps*-HppE was determined to be post-translationally modified by the hydroxylation of a putative active site tyrosine (Tyr95). Analysis of the Fe(II) center by EPR spectroscopy using NO as a spin probe and molecular oxygen surrogate reveals that *Ps*-HppE's metal center is similar, but not identical, to that of *Sw*-HppE. The identity of the rate-determining step for the (*S*)-HPP and (*R*)-HPP reactions was determined by measuring primary deuterium kinetic effects, and the outcome of these results was correlated with density functional theory calculations. Interestingly, the reaction using the nonphysiological substrate (*R*)-HPP was 1.9 times faster than that with (*S*)-HPP for both *Ps*-HppE and *Sw*-HppE. This is likely due to the difference in bond dissociation energy of the abstracted hydrogen atom for each respective reaction. Thus, despite the low level of amino acid sequence identity, *Ps*-HppE is a close mimic of *Sw*-HppE, representing a second example of a non-heme iron-dependent enzyme capable of catalyzing dehydrogenation of a secondary alcohol to form a new C−O bond.

Fosfomycin (**1**) is a clinically useful antibiotic (*1*) for the treatment of limb-threatening diabetic foot infections (*2*) and lower urinary tract infections. It has been shown to be effective against ciprofloxacin-resistant *Escherichia coli* (*3*), as well as methicillin-resistant (*4*) and vancomycin-resistant (*5*) strains of *Staphylococcus aureus*. The antimicrobial activity of fosfomycin is due to the inactivation of UDP-Glc*N*Ac-3-*O*-enolpyruvyltransferase (MurA), which catalyzes the first committed step in the biosynthesis of peptidoglycan, the main component of the bacterial cell wall (*6, 7*).

Fosfomycin belongs to a steadily growing family of natural products containing a C−P bond (*8, 9*). Members of this family, which include fosmydomicin (*10*) and bialaphos (*11*), are all derived from phosphoenolpyruvate (PEP,[1] **2**). The C−P bonds in these compounds are formed through an intramolecular rearrangement reaction catalyzed by PEP mutase, resulting in the conversion of PEP (**2**) to phosphopyruvate (PnPy, **3**) (Figure 1) (*12–14*). Since the equilibrium

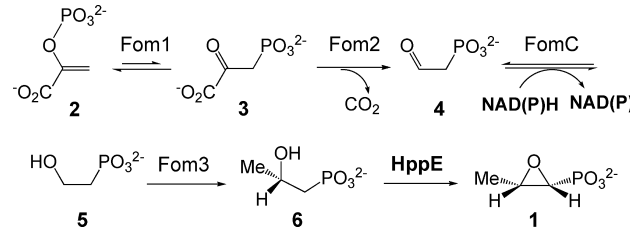

FIGURE 1: Fosfomycin biosynthetic pathway.

[†] This work was supported in parts by NIH Grants GM40541 to H.-w.L. and GM069618 to A.L. and National Institutes of Heath Fellowship GM082085 awarded to S.O.M.

* To whom correspondence should be addressed. Phone: (512) 232-7811. Fax: (512) 471-2746. E-mail: h.w.liu@mail.utexas.edu.

[‡] University of Texas.

[§] Current address: Department of Chemistry, University of California, Berkeley, CA 94720.

[||] Current address: Immunomedics, Inc., 300 American Rd., Morris Plains, NJ 07950.

[⊥] Current address: Genomics Institute of Novartis Research Foundation, 10675 John Jay Hopkins Dr., San Diego, CA 92121.

[@] Current address: Department of Biochemistry and Biophysics, University of California, San Francisco, CA 94143-2532.

[▽] Georgia State University.

[1] Abbreviations: CAS, clavaminic acid synthase; DBE, dissociation bond energy; DFT, density functional theory; DOPA, L-3,4-dioxyphenylalanine; DTT, dithiothreitol; EDTA, ethylenediaminetetraacetic acid; EPR, electron paramagnetic resonance; FMN, flavin mononucleotide; FPLC, fast protein liquid chromatography; HPP, 2-hydroxypropylphosphonic acid; HppE, (*S*)-2-hydroxypropylphosphonic acid epoxidase; H6H, hyoscyamine 6β-hydroxylase; IPTG, isopropyl β-D-thiogalactoside; α-KG, α-ketoglutaric acid; KIE, kinetic isotope effect; LB, Luria-Bertani; NADH, β-nicotinamide adenine dinucleotide, reduced form; $NADP^+$, β-nicotinamide adenine dinucleotide phosphate; NO, nitric oxide; PCR, polymerase chain reaction; PEP, phosphoenolpyruvate; PnPy, phosphopyruvate; SDS−PAGE, sodium dodecyl sulfate−polyacrylamide gel electrophoresis; Tris, tris(hydroxymethyl)aminomethane.

10.1021/bi800877v CCC: $40.75
Published on Web 07/26/2008

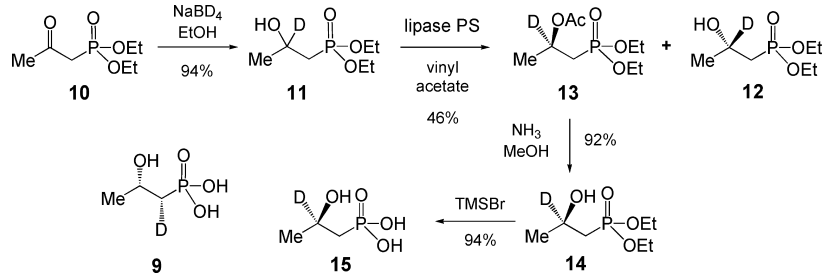

FIGURE 2: Structure of (1*R*,2*S*)-1-[^{2}H]HPP (**9**) and the synthetic scheme for (*R*)-2-[^{2}H]HPP (**15**).

between PEP and PnPy favors PEP, the decarboxylation catalyzed by the second enzyme in the biosynthetic pathway, PnPy decarboxylase, provides the driving force to shift the equilibrium toward C−P bond formation (*15*). The next two steps in the pathway have not been explicitly demonstrated, but they are believed to involve reduction of the aldehyde (**4**) to generate hydroxyethylphosphonic acid (**5**), followed by an unusual methyl transfer reaction to generate (*S*)-2-hydroxypropylphosphonic acid [**6**, (*S*)-HPP] (*16*). The final step of the pathway is the conversion of (*S*)-HPP to fosfomycin (**1**) catalyzed by (*S*)-HPP epoxidase (HppE).

Previous investigations of HppE from *Streptomyces wedmorensis* (*Sw*-HppE) revealed that it is a mononuclear non-heme iron-containing enzyme, and unlike those of most other enzymes in the same class, the activity is α-ketoglutarate-independent (*17*). HppE requires reducing equivalents (e.g., NADH and FMN) and O_2 for activity (*18*). In nature, most epoxide rings are generated via oxidation of the corresponding alkenes by either heme-dependent cytochrome P450s (*19, 20*) or non-heme iron-dependent monooxygenases (*21*). However, isotope labeling experiments with *Sw*-HppE revealed that no oxygen atoms from O_2 are incorporated into fosfomycin. Instead, the oxygen atom of the epoxy ring in **1** is derived from the secondary hydroxyl group of (*S*)-HPP (**6**) (*17, 18*). Thus, the conversion of **6** to **1** by *Sw*-HppE is effectively a dehydrogenation reaction, not a dehydration−oxygenation reaction.

Clearly, *Sw*-HppE is different from all other mononuclear non-heme iron-dependent enzymes in regard to the components it requires for catalytic activity and its unusual epoxidation mechanism. Interestingly, a homologous gene (*orf3*) has been identified in the genome of *Pseudomonas syringae* PB-5123 (*22*). Whether the encoded protein (*Ps*-HppE) is a functional mimic of *Sw*-HppE, acting as an iron-dependent enzyme and catalyzing the analogous epoxidation reaction, has not been investigated. Reported herein are a full account of the biochemical and spectroscopic characterization of the *Ps*-HppE enzyme and the implications for its mode of action.

EXPERIMENTAL PROCEDURES

General. Protein concentrations were determined by the procedure of Bradford using bovine serum albumin as the standard (*23*). NMR spectra were acquired on a Varian Unity 300 spectrometer, and chemical shifts (δ, in parts per million) are given relative to appropriate solvent peaks (for ^{1}H and ^{13}C) and aqueous 85% H_3PO_4 (external, for ^{31}P), with coupling constants reported in hertz. UV−visible absorption spectra were recorded on an Agilent 8453A diode array spectrophotometer. HPLC assays were conducted on the Beckman Coulter System Gold 125 Solvent Module coupled with a System Gold 508 autosampler. The Corona charged aerosol detector (CAD) from ESA (Chelmsford, MA) was used as the HPLC detector.

Materials. Culture medium ingredients were purchased from Difco (Detroit, MI). DNA minipreps were performed using the QIA Spin Miniprep Kit from Qiagen (Valencia, CA). All oligonucleotide primers for PCR amplification of the desired inserts were prepared by Integrated DNA Technologies (Coralville, IA) and used without further purification. Restriction endonucleases were acquired from New England Biolabs (Ipswich, MA). The pET24b(+) vector and the overexpression host strain, *E. coli* BL21(DE3), were obtained from Novagen Inc. (Madison, WI). Electrophoretic materials were products of Gibco BRL or Bio-Rad (Hercules, CA). All chemicals were analytical grade or the highest quality commercially available. Biochemicals, including fosfomycin disodium salt (**1**) standard, were purchased from Sigma-Aldrich Chemical Co. (St. Louis, MO), unless noted otherwise. The physiological substrate, (*S*)-2-hydroxypropylphosphonic acid [(*S*)-HPP (**6**)], and its enantiomer [(*R*)-HPP (**7**)] were chemically synthesized according to a literature procedure (*24*). The deuterium-labeled substrate, (1*R*,2*S*)-1-[^{2}H]HPP (**9**), was synthesized as described previously (*25*).

*Synthesis of (R)-[2-^{2}H]-2-Hydroxypropylphosphonic Acid (**15**). (i) Diethyl [2-^{2}H](2-Hydroxypropyl)phosphonate (**11**).* Sodium borodeuteride (0.35 g, 8 mmol, 0 °C) was slowly added to a solution of diethyl (2-oxopropyl)phosphonate (**10**) (1.5 g, 7.7 mmol) in ethanol (10 mL). After the mixture had been stirred for 2 h, 0.1 g of D_2O was added and the resultant solution was stirred for an additional 10 min. The solvent was removed under reduced pressure. The residue was dissolved in 100 mL of $CHCl_3$, washed three times with 1 M HCl (20 mL), and dried with $MgSO_4$. The solvent was removed under reduced pressure to yield **11** in 94% yield: ^{1}H NMR (300 MHz, $CDCl_3$) δ 4.4 (4H, m), 3.84 (1H, br), 1.85 (2H, d, J = 17.4), 1.26 (6H, m), 1.20 (3H, s); ^{13}C NMR (75 MHz, D_2O) δ 61.8 (t, J = 21.4), 61.7, 61.6, 34.9 (d, J = 137.5), 24.0 (d, J = 16.5), 16.2 (d, J = 5.9); ^{31}P NMR (121 MHz, D_2O) δ 31.1 (s).

*(ii) Diethyl (R)-[2-^{2}H](Acetoxypropyl)phosphonate (**13**).* A mixture of **11** (1.3 g, 6.6 mmol), vinyl acetate (40 mL), isopropyl ether (60 mL), and lipase PS (1 g, Amano Co.) was shaken for 5 days at 30 °C. The mixture was filtered through a short Celite column. The solvent was removed under reduced pressure, and the residue was chromatographed on silica gel (1:1 ethyl acetate/hexanes, 1:0.1 ethyl acetate/ethanol) to afford **13** as a colorless oil in 46% yield: ^{1}H NMR ($CDCl_3$, 300 MHz) δ 4.05 (4H, q, J = 6), 2.12

(1H, d, $J = 19.0$), 1.97 (1H, d, $J = 19.0$) 1.97 (3H, s), 1.26 (9H, m); ^{13}C NMR (75 MHz, $CDCl_3$) δ 170.0, 65.8 (d, $J =$ 23.1), 61.8 (d, $J = 2.3$), 61.7 (d, $J = 2.7$), 32.3 (d, $J = 140.3$), 21.0 (d, $J = 11.0$), 16.2 (d, $J = 6.1$); ^{31}P NMR (121 MHz, D_2O) δ 27.7 (s).

*(iii) Diethyl (R)-[2-^{2}H](2-Hydroxypropyl)phosphonate (***14***).* A solution of **13** (0.6 g, 2.5 mmol) in NH_3/MeOH (2 M, 20 mL) was stirred for 48 h at room temperature. The solvent was removed under reduced pressure, and the residue was chromatographed on silica gel (1:1 ethyl acetate/hexanes, 1:0.1 ethyl acetate/ethanol) to afford **14** as a colorless oil in 92% yield: ^{1}H NMR (300 MHz, $CDCl_3$) δ 4.05 (4H, m), 3.77 (1H, br), 1.87 (2H, d, $J = 21.0$), 1.19 (9H, m); ^{13}C NMR (75 MHz, D_2O) δ 61.7 (t, $J = 23.1$), 61.5, 61.4, 34.9 (d, $J = 137.5$), 24.0 (d, $J = 15.9$), 16.2 (d, $J = 6.0$); ^{31}P NMR (121 MHz, D_2O) δ 31.01 (s).

*(iv) (R)-[2-^{2}H]-2-Hydroxypropylphosphonic Acid (***15***).* A solution of **14** (0.3 g, 1.5 mmol), trimethylsilyl bromide (1 g, 6.5 mmol), and allyltrimethylsilane (0.25 g, 2.1 mmol) in 20 mL of CH_2Cl_2 was refluxed for 6 h under N_2. The solvents were removed in vacuo, and the residue was vigorously stirred with 5 mL of water for 10 min. The aqueous solution was neutralized with ammonium bicarbonate, washed three times with chloroform (10 mL), and lyophilized to give **15** as a white powder in 94% yield: ^{1}H NMR (300 MHz, D_2O) δ 1.41 (2H, d, $J = 17.1$), 0.90 (3H, s); ^{13}C NMR (75 MHz, D_2O) δ 63.9 (t, $J = 22.3$), 37.5 9 (d, $J = 129.3$) 23.2 (d, $J = 8.2$); ^{31}P NMR (D_2O) δ 22.6; high-resolution MS (CI) calcd for $C_3H_8{}^2HO_4P$ 142.3079, found 142.0378.

Construction of the Expression Plasmid for the Ps-HppE Gene. A clone of the *Ps*-HppE gene (*orf3*) in pUC118 was generously provided by H. Seto and T. Kuzuyama from the University of Tokyo (Tokyo, Japan). The *Ps*-HppE gene was amplified from this plasmid using polymerase chain reaction (PCR) and ligated into pET24b(+) to generate pLH01. The resulting plasmid was used to transform *E. coli* BL21(DE3). The general methods and protocols for recombinant DNA manipulations were followed as described by Sambrook et al. (*26*).

Growth of E. coli BL21(DE3)/pLH01 Cells. A 24 mL overnight culture of *E. coli* BL21(DE3)/pLH01 grown at 37 °C in LB medium supplemented with kanamycin (50 μg/mL) was used to inoculate six 1 L flasks containing the same medium. The culture grew at 37 °C until the OD_{600} reached 0.6. The incubation temperature was then lowered to 18 °C, and isopropyl β-D-thiogalactoside (IPTG) was added to a final concentration of 0.5 mM. After incubation for an additional 16 h at 18 °C, cells were harvested by centrifugation (7000*g* for 8 min) at 4 °C and washed with lysis buffer [20 mM Tris-HCl (pH 7.5), 0.1 mM DTT, and 10 mM EDTA]. The washed cells were again centrifuged (7000*g* for 8 min) and stored at −80 °C for future use.

Purification of Recombinant Ps-HppE. All purification operations were carried out at 4 °C except for the fast protein liquid chromatography (FPLC) step. All buffers were degassed and saturated with nitrogen before use. Thawed cells were resuspended in a 5-fold (w/v) excess of lysis buffer (see above) and subjected to 14 × 30 s ultrasonic bursts, with a 50 s cooling interval between each blast. Cellular debris was removed by centrifugation at 17000*g* for 25 min. The supernatant was fractionated by ammonium sulfate precipitation, and the 10−65% ammonium sulfate precipitate was collected by centrifugation. The protein pellet was resuspended in a minimal amount of buffer A [20 mM Tris-HCl (pH 7.5), 0.1 mM DTT, and 0.1 mM EDTA]. The resulting protein solution was dialyzed against 1 L of the same buffer for a total of 3 h with two buffer changes.

The dialysate was applied to a DEAE-Sepharose CL-6B column (6 cm × 18 cm) pre-equilibrated with buffer A. After being loaded, the column was washed with 300 mL of buffer A containing 180 mM NaCl. The elution was then continued with a linear gradient of NaCl from 180 to 300 mM in the same buffer (2 L total volume). The flow rate was 1.5 mL/min, and 20 mL fractions were collected throughout the gradient elution. The fractions containing HppE (as determined by SDS−PAGE) were pooled, concentrated to approximately 15 mL by ultrafiltration on an Amicon concentrator using a YM 10 membrane (Millipore, Bedford, MA), and desalted via dialysis against 1 L of buffer A for 1 h, followed by 1 L of 20 mM Tris-HCl buffer (pH 7.5) for a total of 2 h with one buffer change. After dialysis, the protein was further purified at room temperature by FPLC using a Mono Q HR 16/10 column (GE Healthcare, Piscataway, NJ) and solvent systems B [20 mM Tris-HCl buffer (pH 7.5)] and C (B with 0.6 M NaCl). The elution profile included a linear gradient from 0 to 35% C over 40 mL, followed by a linear gradient from 35 to 60% C over 160 mL, and concluded with a 40 mL wash at 100% C. The flow rate was 7 mL/min, and the detector was set at 280 nm. A peak with a retention time of approximately 19 min was collected, concentrated by ultrafiltration as described before, and dialyzed against 1 L of 20 mM Tris-HCl buffer (pH 7.5) for a total of 3 h with two buffer changes. The purified protein was then divided into aliquots, which were flash-frozen and stored at −80 °C.

Molecular Mass Determination. The molecular mass of *Ps*-HppE was estimated by size exclusion chromatography, performed on a FPLC Superdex 200 HR 10/300 column (GE Healthcare) with an eluent of 20 mM Tris-HCl and 0.15 M NaCl (pH 7.5) and a flow rate of 1 mL/min. Calibration of the column was achieved using the following protein standards (Aldrich): cytochrome *c* (14.2 kDa), carbonic anhydrase (29 kDa), bovine serum albumin (66 kDa), alcohol dehydrogenase (150 kDa), and β-amylase (200 kDa). The void volume (V_0) of the column was measured using blue dextran (2000 kDa). A linear fit to a plot of the logarithm of the molecular mass versus V_e/V_0 was used to estimate the native molecular mass (M_r) of the protein sample, where V_e is the elution volume of the protein standards (*27*).

Iron Titration. Protein samples (1 mL each) for iron titration analysis (*28*) were prepared by mixing with 500 μL of reagent A (1:1 4.5% $KMnO_4$/1.2 N HCl) and incubated at 60 °C for 2 h. To these samples was added 100 μL of reagent B (8.8 g of ascorbic acid, 9.7 g of ammonium acetate, 80 mg of ferrozine, 80 mg of neocuprione, and ddH_2O to a total volume of 25 mL) followed by immediate vortexing. The samples were read at 562 nm after the color was fully developed by a 1 h incubation period at room temperature.

NBT Staining of Ps-HppE. Detection of the presence of quinoid structure in *Ps*-HppE was performed according to a published procedure (*29, 30*). Briefly, the *Ps*-HppE was subjected to 15% SDS−PAGE and transblotted onto a nitrocellulose membrane at 100 V for 1 h using a transfer buffer (25 mM Tris base, 192 mM glycine, and 20%

methanol). Detection of the presence of quinoid structure was performed by immersing the membrane in a solution of 0.24 mM nitroblue tetrazolium and 2 M potassium glycinate (pH 10) for 45 min. After the membrane was rinsed with H_2O, the stained bands were recorded.

Enzyme Activity Assay. The enzyme activity was determined with an HPLC assay, which was carried out as previously described (*31*). However, due to differences in turnover rate, the concentrations of enzyme, iron, and FMN used in the assays for *Ps*-HppE were twice that of *Sw*-HppE. The final concentration of each reagent in a 50 μL reaction was as follows: *Ps*-HppE (100 μM), $Fe(NH_4)_2(SO_4)_2$ (100 μM), FMN (150 μM), (*S*)-HPP (**6**) (10 mM), and NADH (16 mM) in 20 mM Tris-HCl buffer (pH 7.5). To facilitate comparison of the activity of *Ps*-HppE to that of *Sw*-HppE, the assays were carried out on the same day and with the same stock of reagents. The final concentrations in the 50 μL *Sw*-HppE reaction mixtures were 50 μM *Sw*-HppE, 50 μM $Fe(NH_4)_2(SO_4)_2$, 75 μM FMN, 10 mM (*S*)-HPP (**6**), and 16 mM NADH in 20 mM Tris-HCl buffer (pH 7.5). The amount of product formed at each time point was normalized by dividing it by the concentration of HppE and plotted versus time to determine k_{obs}. With the assumption that substrate is saturating, k_{obs} will equal k_{cat}. Over the time scale used in all assays, the product formation was linear with respect to time.

Primary ^{2}H Kinetic Isotope Effect. The catalytic rate of HppE increases with an increase in the concentration of FMN. To determine the FMN:*Ps*-HppE ratio at which the increase in rate saturates, the reaction with (*R*)-HPP (**7**) was conducted at varying concentrations of FMN. Each 50 μL reaction mixture contained 100 μM *Ps*-HppE, 100 μM $Fe(NH_4)_2(SO_4)_2$, 10 mM (*R*)-HPP, 16 mM NADH, and 0.01−12.9 mM FMN in 20 mM Tris-HCl buffer (pH 7.5). Each reaction mixture was incubated at room temperature for 20 min before the reaction was quenched with 50 μL of 2 M acetic acid and analyzed by HPLC as previously described (*31*). The concentration of ketone product (**8**) formed was plotted versus the FMN:*Ps*-HppE ratio to determine the saturating ratio. The minimum saturating ratio was determined to be 50:1 (FMN:*Ps*-HppE). It was assumed that the saturating FMN:*Ps*-HppE ratio for the (*S*)-HPP (**6**) reaction was the same as that determined for the (*R*)-HPP (**7**) reaction. To ascertain the primary ^{2}H KIE for hydrogen atom abstraction, k_{obs} was determined using the HPLC assay with (*S*)-HPP (**6**), (1*R*,2*S*)-1-[^{2}H]HPP (**9**), (*R*)-HPP (**7**), or (*R*)-2-[^{2}H]HPP (**15**) at a 50:1 FMN:*Ps*-HppE ratio. The final concentrations in the 50 μL reaction mixture used to determine the KIEs were 100 μM *Ps*-HppE, 100 μM $Fe(NH_4)_2(SO_4)_2$, 5 mM FMN, 10 mM HPP (**6**, **9**, **7**, or **15**), and 16 mM NADH in 20 mM Tris-HCl buffer (pH 7.5).

NMR Characterization of Ps-HppE's Products. ^{1}H and ^{31}P NMR spectroscopy were used to characterize the products of the reaction catalyzed by *Ps*-HppE with (*S*)-HPP (**6**) and (*R*)-HPP (**7**) as the substrate. The following conditions were used: 150 μM *Ps*-HppE, 150 μM $Fe(NH_4)_2(SO_4)_2$, 370 μM FMN, 40 mM (*S*)-HPP (**6**) or (*R*)-HPP (**7**), and 40 mM NADH in 200 μL of 20 mM Tris-HCl buffer (pH 7.5). The reaction mixtures were incubated at room temperature for 15 h. The samples were then lyophilized to dryness and redissolved in 600 μL of D_2O. Spectral data of the product of the (*S*)-HPP reaction (fosfomycin, **1**): ^{1}H NMR (300 MHz, D_2O) δ 3.11 (1H, m, J = 5.4, 2-H), 2.66 (1H, d, J = 5.3, 18.6, 1-H), 1.33 (3H, d, J = 5.4, 3-H); ^{31}P NMR (121 MHz, D_2O) δ 10.9 (s). Spectral data for the product of the (*R*)-HPP reaction (2-oxopropylphosphonic acid, **8**): ^{1}H NMR (300 MHz, D_2O) δ 2.81 (2H, d, J = 21.0), 2.16 (3H, s); ^{31}P NMR (121 MHz, D_2O) δ 11.1 (s).

Effects of Metal Ions on the Activity of Ps-HppE. A systematic investigation of the metal ion requirement for the activity of *Ps*-HppE was performed by incubating enzyme with different redox-active metals, such as iron [$Fe(NH_4)_2(SO_4)_2$], copper ($CuSO_4$), cobalt ($CoCl_2$), and manganese ($MnCl_2$), or the non-redox-active metal, zinc ($ZnSO_4$), and assessing their effects on enzyme activity. A typical 50 μL reaction mixture contained 16 mM NADH, 10 mM (*S*)-HPP (**6**), 100 μM *Ps*-HppE, 150 μM FMN, and the metal under investigation (at 100 μM) in 20 mM Tris-HCl buffer (pH 7.5). After the mixture had been incubated at room temperature for 1.5 h, the reaction was quenched with 2 M acetic acid, and the relative activity of each sample was determined by the HPLC assay described above. To further assess the metal ion requirement for enzyme activity, the effect of the metal chelator, EDTA, on *Ps*-HppE catalysis was also examined. In this case, the activity assay with *Ps*-HppE reconstituted with ferrous iron was repeated in the presence of 5 mM EDTA.

Dependence of Ps-HppE Activity on Oxygen. In a sealed vessel, an assay mixture (1 mL) containing 200 μM *Ps*-HppE and 200 μM $Fe(NH_4)_2(SO_4)_2$ in 20 mM Tris-HCl (pH 7.5) was made anaerobic by 15 repeated cycles of subjecting the mixture to vacuum and purging with argon. The mixture was kept under argon for 20 min followed by another 15 cycles of vacuum and argon purging to ensure anaerobic conditions. In a separate sealed vessel, a solution of 32 mM NADH, 300 μM FMN, and 20 mM (*S*)-HPP (**6**) in the same buffer was made anaerobic by the same procedure. The vessels were transferred to an anaerobic glovebox, where 25 μL of each mixture was combined to start the assay. The final concentrations of reagents in a 50 μL reaction mixture were 100 μM *Ps*-HppE, 100 μM $Fe(NH_4)_2(SO_4)_2$, 150 μM FMN, 10 mM (*S*)-HPP, and 16 mM NADH. After the mixture had been incubated for 1.5 h at room temperature, the reaction was quenched with 50 μL of 2 M acetic acid. The activity was then analyzed by the HPLC assay described above.

DFT Calculations of Bond Dissociation Energies. To gain insight into the distinct regiospecificity observed in the reactions of HppE with (*R*)- and (*S*)-HPP (**7** and **6**, respectively), electronic structure calculations were performed to estimate the bond dissociation enthalpies of the C_1−H and C_2−H bonds of HPP. All calculations were performed using Gaussian98 (*32*). Geometry optimizations were performed using Becke-style three-parameter density functional theory (DFT) with the Lee−Yang−Parr correlation functional (B3LYP) and Pople's diffuse polarized triple-ζ 6-311+G(d,p) basis set, with the Opt = Tight and Int = Ultrafine keywords. The initial geometry of the heavy atoms of the substrate was taken from the crystal structure of *Sw*-HppE in complex with (*S*)-HPP (**6**) and ferrous iron (PDB entry 1ZZ8) (*33*). Vibrational frequency calculations were then performed on the optimized geometries using the same B3LYP/6-311+G(d,p) scheme at 25 °C and 1.0 atm, with a scale factor of 0.9877 to correct the zero-point vibrational energies (*34*).

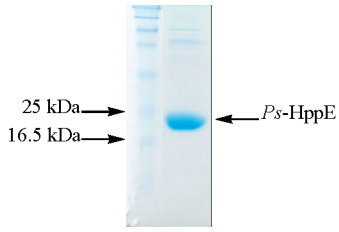

FIGURE 3: SDS−PAGE of as-isolated *Ps*-HppE.

EPR Spectroscopy. X-Band EPR spectra of *Ps*-HppE−Fe(II) nitrosyl complexes in the presence and absence of substrate (**6**) were collected using a Bruker (Billerica, MA) EMX spectrometer with a 4119HS high-sensitivity resonator. The sample temperature was maintained with an ITC503S temperature controller, an ESR910 liquid helium cryostat, and an LLT650/13 liquid helium transfer tube (Oxford Instruments, Concord, MA). The EPR parameters were obtained by simulation of the experimental spectra using an EPR program written by F. Neese (*35*) and further verified in Bruker SimFonia. The as-isolated *Ps*-HppE was made anaerobic by repeated cycles of evacuation and flushing with argon. A molar equivalent of $Fe(NH_4)_2(SO_4)_2$ from an anaerobic stock solution was added to *Ps*-HppE to reconstitute it under anaerobic conditions. For the sample with (*S*)-HPP bound, 10 molar equiv of anaerobic (*S*)-HPP (**6**) was incubated with the ferrous-reconstituted *Ps*-HppE. Nitric oxide gas was passed over NaOH pellets to remove any acid impurities and then introduced into the enzyme samples through a gastight Hamilton syringe. The samples were then frozen by slow immersion in liquid nitrogen for later EPR analysis. Spin quantitation was performed by double integration of the EPR signal recorded under nonsaturating conditions at 20 K and comparison with a Cu-EDTA standard (0.5 mM).

RESULTS

Cloning, Overexpression, and Purification of Ps-HppE. The gene, *orf3*, encoding *Ps*-HppE (*22*) was amplified by PCR and cloned into the pET24b(+) expression vector. The resulting construct, pLH01, was used to transform *E. coli* BL21(DE3) cells. The induction of *orf3* expression by IPTG was conducted at 18 °C to minimize the formation of inclusion bodies. As shown by SDS−PAGE (Figure 3), the desired protein was isolated in nearly homogeneous form after ammonium sulfate fractionation and two anion exchange chromatographic steps (DEAE-Sepharose and MonoQ). The subunit molecular mass of 21 kDa, assessed by SDS−PAGE, correlates well with the predicted value of 21315 Da calculated from the deduced amino acid sequence. As determined by size exclusion chromatography, the purified recombinant *Ps*-HppE has a mass of 73 kDa in solution (9 kDa higher than that predicted for a homotrimer). When *Sw*-HppE, which has a subunit molecular mass of 21210 Da, was analyzed under the same conditions, it yielded a mass of 95 kDa (10 kDa higher than that predicted for a homotetramer). On the basis of the results of X-ray crystallography, *Sw*-HppE has been determined to exist as a homotetramer (*33*). Thus, these results suggest that *Ps*-HppE likely exists as a homotrimer instead of a homotetramer in solution. Determination of the crystal structure for *Ps*-HppE is in progress, and the results will provide additional information about the oligomerization state of the enzyme.

Sequence Analysis. Though *S. wedmorensis* and *P. syringae* are both fosfomycin producers, amino acid sequence alignment showed that their respective HppEs share only 27% sequence identity (Figure 4). However, the residues that have been determined to be crucial for *Sw*-HppE catalysis are conserved in *Ps*-HppE. These include Lys21, Tyr92, Tyr93, Tyr95, His128, Glu132, and His171 (*Ps*-HppE numbering). The later three residues are assigned as the ligands responsible for iron binding in *Ps*-HppE, since the corresponding residues (His138, Glu142, and His180) in *Sw*-HppE have been determined to be the metal binding residues (*33, 36*). The proposed role for Lys21 in *Ps*-HppE is to stabilize the negative charge on the iron−superoxo intermediate generated during oxygen activation. A similar function has been assigned to its counterpart, Lys23, in *Sw*-HppE, based on the crystal structure as well as mutagenesis results (*33*). The three conserved tyrosine residues (Tyr92, Tyr93, and Tyr95) are proposed to be part of a relay system for shuttling reducing equivalents into the enzyme active site. This is based on crystallographic studies in which *Sw*-HppE was found to undergo a significant conformational change upon (*S*)-HPP binding, which aligns the tyrosine residues in a row constituting a pathway extending from the surface of the protein to the active site iron (*33*).

Reconstitution of Epoxidase Activity. As described above, *Ps*-HppE and *Sw*-HppE are thought to catalyze the same reaction, and residues important for catalysis are conserved in both enzymes. Thus, it is likely that *Ps*-HppE utilizes the same chemistry as *Sw*-HppE to catalyze epoxide ring formation. To verify this hypothesis, the as-purified *Ps*-HppE was reconstituted with ferrous iron and assayed under aerobic conditions in the presence of FMN, NADH, and (*S*)-HPP (using the same procedures developed for *Sw*-HppE) (*18*). Formation of the product, fosfomycin (**1**), was detected by HPLC, and its chemical identity was confirmed by ^1H and ^{31}P NMR spectroscopy. If either iron, FMN, or NADH was omitted from the reaction mixture, no product formation was detected by HPLC. These results indicate that NADH is essential for catalysis, consistent with its proposed role of providing the reducing equivalents needed for oxygen activation and the conversion of molecular oxygen to water (Figure 5). The requirement of FMN may be ascribed to its role as an electron mediator in the reduction of the metal center by NADH. Additionally, when the reactions were carried out under anaerobic conditions, no epoxidase activity could be detected by the HPLC-based enzyme assay, indicating that O_2 is required for turnover.

In previous studies, *Sw*-HppE was found to catalyze the conversion of (*R*)-HPP (**7**) to 2-oxopropylphosphonic acid (**8**) (*37*). Further investigation indicated that the stereochemistry at the C_2 position of HPP determines the regiospecificity of the initial hydrogen atom abstraction. As depicted in Figure 5, when (*S*)-HPP binds to *Sw*-HppE, the C_1 *pro-R* hydrogen atom is abstracted, leading to the production of fosfomycin. However, when (*R*)-HPP binds to *Sw*-HppE, it is thought that the C_2 hydrogen atom is abstracted, which leads to the formation of 2-oxopropylphosphonic acid (Figure 6). It was investigated if the stereochemistry of the substrate also controls the regiospecificity of the initial hydrogen atom abstraction in the *Ps*-HppE-catalyzed reaction. When the

```
Sw-HppE      1    MSNTKTASTGFAELLKDRREQVKMDHAALASLLGETPETVAAWENGEGGELTLTQLGRIA
Ps-HppE      1    M-DVRTLAVGKAHLEA-LLATRKMT---LEHLQDVRHDATQVYFDG------LEHLQNVA
Consensus              T   G A L        KM    L  L              G      L  L   A

Sw-HppE     61    HVLGTSIGALTP-PAGNDLDDGVIIQMPDERPILKGVRDNVDYYVYNCLVRTKRAPSLVP
Ps-HppE     50    QYLAIPLSEFFVGQTQSDLDDGVKIARRNGGFKREEIRGGVHYYTYEHLVTTNQDPGLMA
Consensus             L              DLDDGV I            R  V YY Y  LV T   P L

Sw-HppE    120    LVVDVLTDNPDDAKFNSGHAGNEFLFVLEGEIHMKWG-DKENPKEALLPTGASMFVEEHV
Ps-HppE    110    LRLDLHSDDEQPLRLNGGHGSREIVYVTRGAVRVRWVGDNDELKEDVLNEGDSIFILPNV
Consensus          L  D   D       N GH   E   V  G     W  D    KE  L  G S F    V

Sw-HppE    179    PHAFTAAKGTGSAKLIAVNF-
Ps-HppE    170    PHSFTNHVGGAKSEIIAINYG
Consensus          PH FT   G      IA N
```

FIGURE 4: Protein sequence alignment of *Ps*-HppE and *Sw*-HppE.

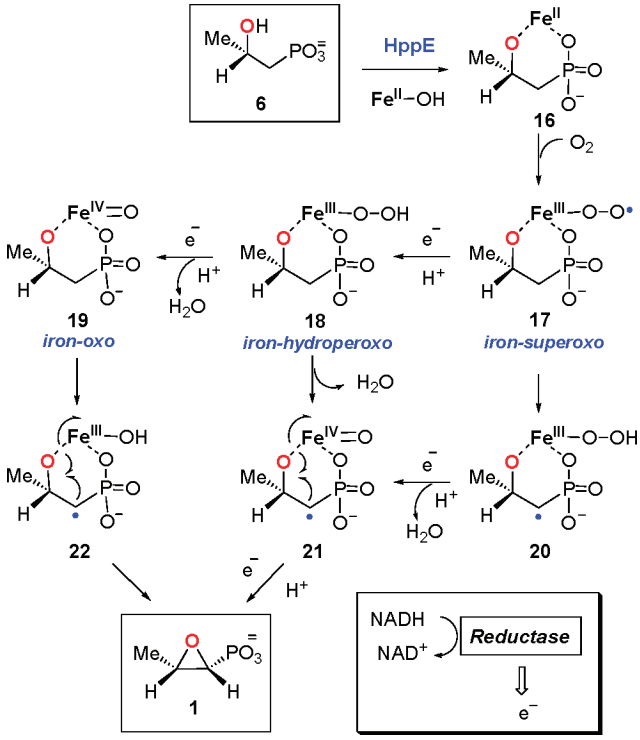

FIGURE 5: Proposed iron-, FMN-, and NADH-dependent HppE mechanism.

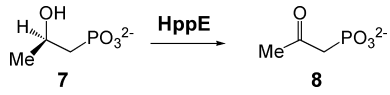

FIGURE 6: HppE-catalyzed reaction with (*R*)-HPP (**7**) as the substrate.

activity assays for *Ps*-HppE described above were conducted using (*R*)-HPP as a substrate, the product 2-oxopropylphosphonic acid was indeed formed as verified by ^{1}H and ^{31}P NMR spectroscopy.

Iron Quantitation and Metal Analysis. The ferrous concentration was determined by the ferrozine method (*28*). Two dilutions of the protein sample (1 mL each) were prepared with concentrations of approximately 1.3 and 2.1 mg/mL in duplicate. The titration analysis, as compared to the standard curve, revealed that the iron content after reconstitution was approximately one iron per HppE monomer. To explore if other redox-active metals could support catalysis, the catalytic properties of *Ps*-HppE reconstituted with cobalt, copper, and manganese were investigated. No turnover could be detected with any of these metals using the epoxidase assay. The fact that the addition of 5 mM EDTA abolished the activity of

Table 1: Rate Constants for HppE Reactions with (*S*)- and (*R*)-HPP[a]

	Ps-HppE	*Sw*-HppE
(*S*)-HPP k_{obs} (min^{-1})	0.17 ± 0.02	0.31 ± 0.06
(*R*)-HPP k_{obs} (min^{-1})	0.33 ± 0.04	0.58 ± 0.02

[a] The reactions were carried out at a FMN:HppE ratio of 1.5:1.

Table 2: Primary Deuterium Kinetic Isotope Effects for *Ps*-HppE with (*R*)- and (*S*)-HPP[a]

substrate	k_{obs} (min^{-1})	$^{D}k_{obs}$
(*S*)-HPP (**6**)	0.46 ± 0.04	
		1.5 ± 0.2
(1*R*,2*S*)-1-[^{2}H]HPP (**9**)	0.31 ± 0.03	
(*R*)-HPP (**7**)	1.12 ± 0.10	
		1.08 ± 0.13
(*R*)-2-[^{2}H]HPP (**15**)	1.04 ± 0.09	

[a] The reactions were carried out at a FMN:HppE ratio of 50:1.

the iron-reconstituted *Ps*-HppE further confirmed the importance of iron in catalysis.

Activity with (S)-HPP and (R)-HPP. To determine how the activity of *Ps*-HppE compares to that of *Sw*-HppE, the rate of catalysis with (*S*)-HPP (**6**) or (*R*)-HPP (**7**) was measured at saturating substrate concentrations (10 mM). As seen in Table 1, the observed rate constants for both enzymes with each substrate are similar in magnitude. Interestingly, *Sw*-HppE is roughly 1.8 times faster than *Ps*-HppE with both (*S*)-HPP and (*R*)-HPP. Thus, it appears that *Sw*-HppE is a more effective epoxidase. Moreover, the reaction rate for (*R*)-HPP (**7**) is approximately 1.9 times faster than that for (*S*)-HPP (**6**) with either *Sw*-HppE or *Ps*-HppE.

To determine how rate-limiting hydrogen atom abstraction is for the *Ps*-HppE-catalyzed reactions with (*S*)-HPP (**6**) and (*R*)-HPP (**7**), primary ^{2}H KIEs were determined (Table 2). It has previously been demonstrated that the C_1 *pro-R* hydrogen atom is abstracted in the conversion of (*S*)-HPP to fosfomycin (*25, 38*); therefore, (1*R*,2*S*)-1-[^{2}H]HPP (**9**) was used as the labeled substrate to determine the ^{2}H KIE. For the turnover of (*R*)-HPP to **8**, it is the C_2 hydrogen atom that is abstracted (*37*), so the ^{2}H KIE was measured using (*R*)-2-[^{2}H]HPP (**15**). It is known that the rate of the HppE-catalyzed reaction increases with an increase in FMN concentration, presumably due to an increased rate of electron transfer to the active site iron. To reduce the commitments to catalysis, which could mask the primary ^{2}H KIEs, the KIEs were measured using a saturating FMN:*Ps*-HppE ratio (50:1). With (*S*)-HPP, the measured primary ^{2}H KIE of 1.5 is smaller than what would be expected for an intrinsic primary ^{2}H KIE; thus, the hydrogen abstraction step is only partially

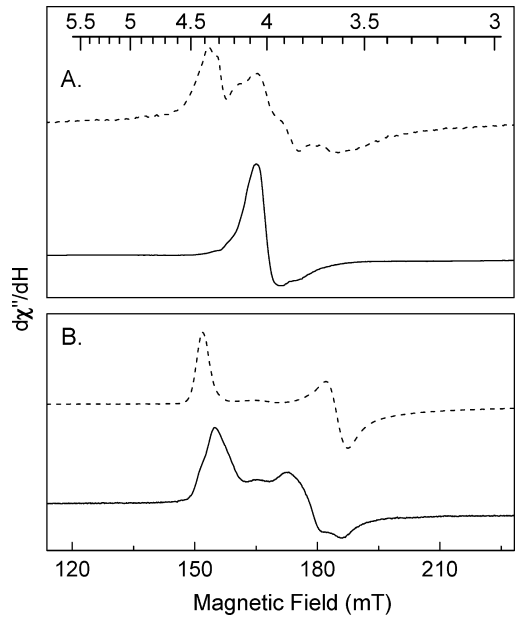

FIGURE 7: EPR spectra of HppE−Fe(II)−nitrosyl complexes at 4 K with the *g* scale plotted above the spectra: (A) 250 μM *Ps*-HppE (—) or *Sw*-HppE (---) in the presence of NO and (B) the substrate−HppE−NO ternary complex [*Ps*-HppE (—) and *Sw*-HppE (---)]. Substrate was present in a 10-fold excess. The *Ps*-HppE spectrum shown in the bottom panel also contains a minor species (ca. 5%) due to a denatured protein-bound Fe−NO complex (g = 4.07), which was previously characterized (*18*). Instrumental conditions: microwave frequency, 9.6 GHz; microwave power, 0.5 mW; modulation amplitude, 5 G; modulation frequency, 100 kHz; time constant, 0.02 s; and sweep rate, 5 mT/s.

rate-limiting. For the (*R*)-HPP reaction, there is a ^{2}H KIE of unity, so hydrogen abstraction is not significantly rate-limiting. In both reactions, electron transfer is presumed to be the predominant rate-limiting step.

The reduced rate and small but significant primary ^{2}H KIE measured for *Ps*-HppE with (*S*)-HPP (**6**) as the substrate imply that hydrogen atom abstraction is slower and more rate-limiting for (*S*)-HPP than for (*R*)-HPP. There are two possible explanations for the difference in rates for C_2 hydrogen atom abstraction in the (*R*)-HPP reaction versus C_1 hydrogen atom abstraction in the (*S*)-HPP reaction. It is conceivable that the C_2 hydrogen of (*R*)-HPP is closer to the reactive oxygen species in the Michaelis complex than is the C_1 hydrogen of (*S*)-HPP, thus reducing the barrier for abstraction. Alternatively, the rate difference could be due to differences in the energetics of the hydrogen being abstracted and the stability of the resulting substrate radical. On the basis of DFT calculations, the bond dissociation energies (BDEs) for the C_1 and C_2 hydrogen atoms are 96.5 and 89.0 kcal/mol, respectively. Thus, the thermodynamic energy barrier for hydrogen atom abstraction in the (*R*)-HPP reaction is 7.5 kcal/mol lower than in the (*S*)-HPP reaction. This may account for the observed rate difference between the two substrates.

EPR Characterization of Ps-HppE. The EPR spectra of the *Ps*-HppE−Fe(II)−nitrosyl complexes, in the presence and absence of substrate, are shown in Figure 7. The corresponding EPR spectra of *Sw*-HppE are also shown in this figure in dashed traces for comparison. In the absence of (*S*)-HPP (**6**), the EPR spectrum of the *Ps*-HppE−Fe(II)−NO complex consists of two signals present in a 9:1 ratio. The major species gives rise to an axial EPR signal for which $g_\perp$ = 3.96 and $g_\parallel$ = 2.00, which is typical for an $S = {}^3/_2$ non-heme {Fe-NO}^{7} species with an *E*/*D* value of 0.01 and a positive *D*. The minor species is also an $S = {}^3/_2$ {Fe-NO}^{7} complex but exhibits a rhombic EPR signal with principal *g* values of 4.30, 3.69, and 2.00 (*E*/*D* value of 0.05). In contrast, two rhombic signals with resonances at g = 4.14, 3.92, and 1.99 (*E*/*D* = 0.013) and g = 4.32, 3.70, and 1.98 (*E*/*D* = 0.055) are observed for *Sw*-HppE in a 3:7 ratio (*18*). Thus, the Fe(II) center in *Ps*-HppE is more axial and uniform than that in *Sw*-HppE.

Although the ferrous center of *Sw*-HppE can react with NO to form two spectroscopically distinguishable complexes, we have previously found that only a single substrate−Fe−NO complex (g = 4.42, 3.63, and 1.97; *E*/*D* = 0.066) is formed in the presence of (*S*)-HPP (**6**) (*18*). These results suggested that the substrate likely binds to the active site iron center first and, in doing so, organizes the center to bind NO, an O_2 analogue, in only one conformation. In contrast, in the presence of (*S*)-HPP, the EPR spectrum of the nitrosyl complex of the *Ps*-HppE−Fe(II) species is heterogeneous. Two sets of EPR signals are observed in a 3:7 ratio, both of which can be attributed to substrate−enzyme−NO ternary complexes. The minor ternary complex (30%) observed for *Ps*-HppE exhibits the same EPR parameters that were previously observed for *Sw*-HppE (g = 4.42, 3.63, and 1.97; *E*/*D* = 0.066). The major ternary complex (70%) is less rhombic, with resonances at g = 4.33, 3.74, and 2.00 (*E*/*D* = 0.059).

These results indicate that substrate and NO can bind to the ferrous center of the reduced *Ps*-HppE enzyme to form a stable complex. However, the heterogeneity observed in the EPR spectrum of the ternary complex of *Ps*-HppE suggests that substrate binds to the active site Fe(II) ion in two different conformations. Our recent isotope labeling study showed that the uniform EPR signal observed for the ternary complex of *Sw*-HppE is a result of coordination of the substrate to the Fe(II) ion in a bidentate fashion (*39*). This same species is also observed with *Ps*-HppE, although it represents only 30% of the total iron. The remaining 70% may be in a form with monodentate coordination of the substrate to the metal center. This is an intermediate step toward bidentate substrate binding to the active site iron.

Post-Translational Hydroxylation of Ps-HppE. The reconstituted ferrous form of *Ps*-HppE is colorless. However, when the protein is exposed to air, it slowly turns green. The optical spectrum of this green protein exhibits a broad absorption band with a λ_{max} at 672 nm and a molar absorption coefficient of approximately 409 (M Fe)$^{-1}$ cm^{-1} (Figure 8). A similar absorption band with a λ_{max} at 680 nm and a molar extinction coefficient of 450 (M Fe)$^{-1}$ cm^{-1} was previously observed when the reconstituted ferrous form of *Sw*-HppE was exposed to air (*18*). Further investigation showed that *Sw*-HppE is post-translationally modified by the hydroxylation of Tyr105 to DOPA (*30*). The green chromophore arises from a ligand to metal charge transfer transition of a bidentate catecholate−Fe(III) complex formed between the active site iron center and the modified tyrosine. To verify the presence of the DOPA in *Ps*-HppE, the as-isolated enzyme was subjected to Paz's quinone staining reagents [glycine and nitroblue tetrazolium (NBT)] (*29*). If a quinone is present, it can oxidize the glycine in solution. The reduced quinone then reacts with dioxygen to generate superoxide,

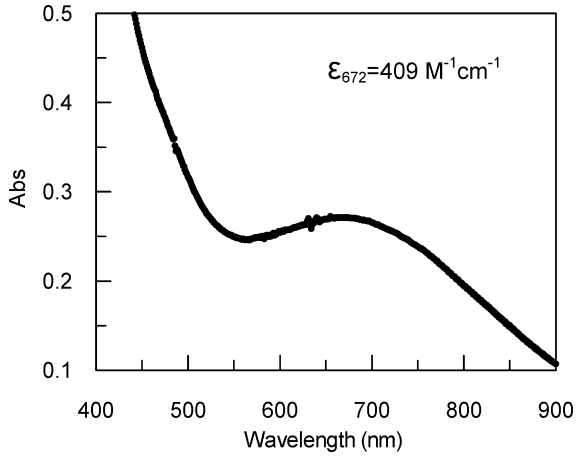

FIGURE 8: Electronic absorption spectrum of *Ps*-HppE [660 μM in 20 mM Tris buffer (pH 7.5)] reconstituted with 1.1 equiv of $Fe(NH_4)_2(SO_4)_2$.

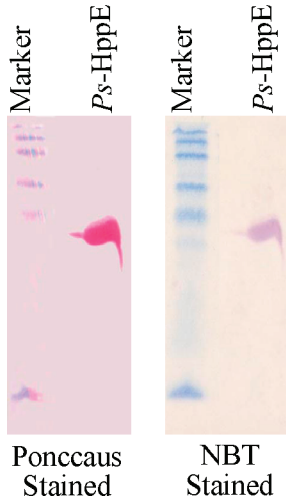

FIGURE 9: SDS−PAGE of as-purified *Ps*-HppE. Protein bands were transferred electrophoretically to a nitrocellulose membrane and temporarily stained for proteins with Ponccaus (left), followed by NBT (right) to detect the presence of quinone (see Experimental Procedures for details).

which oxidizes NBT to generate a bluish-purple compound. As shown in Figure 9, the stain produced a positive result, indicating the presence of quinone in *Ps*-HppE. It is therefore highly likely that Tyr95 (the Tyr105 equivalent in *Ps*-HppE) is post-translationally hydroxylated to DOPA. The significance of this modification in HppE is currently under investigation.

DISCUSSION

In this study, the newly isolated *orf3* gene product from *P. syringae* PB-5123 was established to be a non-heme iron-dependent *Ps*-HppE enzyme that catalyzes the same reactions and requires the same components (iron, FMN, NADH, and O_2) as *Sw*-HppE, despite the sequences of the enzymes being only 27% identical. As implicated by the EPR results, dioxygen is activated in the reaction by ferrous iron, leading to the formation of a reactive species capable of abstracting a hydrogen atom from the substrate. To complete the oxygen reduction, four electrons are consumed. Two of the electrons are supplied by the substrate, and the remaining two are provided by NADH. Due to the fact that the reduction of iron requires single-electron transfer and NADH is an obligate two-electron donor, FMN is required to mediate the transfer of reducing equivalents from NADH to the active site iron. Since no suitable reductase gene can be found in the *S. wedmorensis* and *P. syringae* fosfomycin biosynthetic gene clusters, a promiscuous reductase may serve the role of electron mediator in vivo.

The rate of the *Sw*-HppE-catalyzed epoxidation reaction is consistently 1.8 times faster than that of *Ps*-HppE. On the basis of EPR and crystallographic studies, (*S*)-HPP binds to the active site of *Sw*-HppE and efficiently organizes the iron center such that all of the substrate is coordinated in a bidentate manner. In this conformation, the C_1 *pro-R* hydrogen is ideally positioned to be abstracted by the activated oxygen species. By contrast, only 30% of the iron is found in this activated conformation in *Ps*-HppE, with the remaining likely being bound to substrate via monodentate coordination. The position of this internal equilibrium step for switching between mono- and bidentate substrate coordination may account for the modest differences in rate between *Sw*-HppE and *Ps*-HppE. Also, the rate of HppE-catalyzed oxidation of (*R*)-HPP is consistently 1.9 times faster than the rate of (*S*)-HPP epoxidation. A likely explanation for this difference in rate was obtained from DFT calculations, which showed that the BDE of the C_2 hydrogen of (*R*)-HPP is 7.5 kcal/mol lower than that of the C_1 hydrogen of (*S*)-HPP.

The mechanism of HppE epoxidation (Figure 5) has been proposed to parallel alkane hydroxylation catalyzed by cytochrome P450 (*20*) and non-heme iron-dependent oxygenases (*40, 41*). The reaction likely begins with abstraction of a hydrogen atom from the C_1 position by an activated oxygen species. In a manner similar to the oxygen rebound mechanism for cytochrome P450s, the C_1-centered radical intermediate can then cyclize to form fosfomycin and the reduced iron center. The reactive oxygen species can be one of three intermediates: Fe(III)−superoxo (**17**), Fe(III)−hydroperoxo (**18**), and Fe(IV)−oxo (**19**). Fe(III)−superoxide (**17**), which forms upon dioxygen binding to the ferrous iron center of **16**, has been proposed to be the reactive oxygen species for isopenicillin N synthase (IPNS) (*42, 43*). The Fe(III)−superoxide species can be reduced by one electron and protonated to form Fe(III)−hydroperoxide (**18**), which could also abstract the C_1 hydrogen atom (**18** → **21**). The Fe(III)−hydroperoxide species can also be reduced by a single electron and protonated with concurrent cleavage of the O−O bond to form an Fe(IV)−oxo intermediate (**19**), which can abstract the hydrogen atom (**19** → **22**), as proposed for α-ketoglutarate-dependent TauD (*44*) and tyrosine hydroxylase (*45*).

On the basis of a sequence comparison with *Sw*-HppE, *Ps*-HppE utilizes two histidines and one glutamate residue as ligands to bind the active site iron. Thus, *Ps*-HppE is a new member of the growing superfamily of non-heme iron-dependent enzymes that contain the 2-His-1-carboxylate facial triad to bind and activate iron. Members of this enzyme family have proven to be remarkably versatile in the types of reactions they catalyze (*19*). According to Koehntop et al., this superfamily can be divided into five classes: extradiol-cleaving catechol dioxygenases, Rieske dioxygenases, α-ketoglutarate-dependent enzymes, pterin-dependent enzymes, and "other" oxidases (*46*). The fifth class is a "catch all" for enzymes that cannot be included in one of the other

four classes. This class includes IPNS, 1-aminocyclopropane-1-carboxylic acid oxidase, and HppE.

The method of C−O bond formation catalyzed by HppE is unique in Nature. Coordination of the hydroxyl group of (*S*)-HPP to the active site iron is thought to be critical for the cyclization step. There are two α-KG-dependent enzymes, hyoscyamine 6β-hydroxylase (H6H) (*47*) and clavaminic acid synthase (CAS) (*48*), that catalyze similar C−O bond formations; however, for the standard oxygen activation mechanism in α-KG-dependent enzymes (*41*), there is no available coordination site for the reacting oxygen. It will be interesting to determine if the chemistry utilized by HppE for C−O bond formation is more widely used and what adaptations (if any) are required for its use in α-KG-dependent enzymes catalyzing similar transformations.

ACKNOWLEDGMENT

We thank Professor Haruo Seto (now at Tokyo University of Agriculture, Tokyo, Japan) and Dr. Tomohisa Kuzuyama from the University of Tokyo for the *Ps*-HppE gene.

REFERENCES

1. Itoh, N., Kusaka, M., Hirota, T., and Nomura, A. (1995) Microbial production of antibiotic fosfomycin by a stereoselective epoxidation and its formation mechanism. *Appl. Microbiol. Biotechnol. 43*, 394–401.
2. Stengel, D., Gorzer, E., Schintler, M., Legat, F. J., Amann, W., Pieber, T., Ekkernkamp, A., and Graninger, W. (2005) Second-line treatment of limb-threatening diabetic foot infections with intravenous fosfomycin. *J. Chemother. 17*, 527–535.
3. Ko, K. S., Suh, J. Y., Peck, K. R., Lee, M. Y., Oh, W. S., Kwon, K. T., Jung, D. S., Lee, N. Y., and Song, J. H. (2007) In vitro activity of fosfomycin against ciprofloxacin-resistant or extended-spectrum β-lactamase-producing *Escherichia coli* isolated from urine and blood. *Diagn. Microbiol. Infect. Dis. 58*, 111–115.
4. Nakazawa, H., Kikuchi, Y., Honda, T., Isago, T., and Nozaki, M. (2003) Enhancement of antimicrobial effects of various antibiotics against methicillin-resistant *Staphylococcus aureus* (MRSA) by combination with fosfomycin. *J. Infect. Chemother. 9*, 304–309.
5. Cassone, M., Campanile, F., Pantosti, A., Venditti, M., and Stefani, S. (2004) Identification of a variant "Rome clone" of methicillin-resistant *Staphylococcus aureus* with decreased susceptibility to vancomycin, responsible for an outbreak in an intensive care unit. *Microb. Drug Resist. 10*, 43–49.
6. Marquardt, J. L., Brown, E. D., Lane, W. S., Haley, T. M., Ichikawa, Y., Wong, C. H., and Walsh, C. T. (1994) Kinetics, stoichiometry, and identification of the reactive thiolate in the inactivation of UDP-GlcNAc enolpyruvoyl transferase by the antibiotic fosfomycin. *Biochemistry 33*, 10646–10651.
7. Brown, E. D., Vivas, E. I., Walsh, C. T., and Kolter, R. (1995) MurA (MurZ), the enzyme that catalyzes the first committed step in peptidoglycan biosynthesis, is essential in *Escherichia coli*. *J. Bacteriol. 177*, 4194–4197.
8. Seto, H., and Kuzuyama, T. (1999) Bioactive natural products with carbon-phosphorus bonds and their biosynthesis. *Nat. Prod. Rep. 16*, 589–596.
9. Hidaka, T., Iwakura, H., Imai, S., and Seto, H. (1992) Studies on the biosynthesis of fosfomycin. 3. Detection of phosphoenolpyruvate phosphomutase activity in a fosfomycin high-producing strain of *Streptomyces wedmorensis* and characterization of its blocked mutant NP-7. *J. Antibiot. 45*, 1008–1010.
10. Jomaa, H., Wiesner, J., Sanderbrand, S., Altincicek, B., Weidemeyer, C., Hintz, M., Turbachova, I., Eberl, M., Zeidler, J., Lichtenthaler, H. K., Soldati, D., and Beck, E. (1999) Inhibitors of the nonmevalonate pathway of isoprenoid biosynthesis as antimalarial drugs. *Science 285*, 1573–1576.
11. Hidaka, T., Mori, M., Imai, S., Hara, O., Nagaoka, K., and Seto, H. (1989) Studies on the biosynthesis of bialaphos (SF-1293). 9. Biochemical mechanism of C-P bond formation in bialaphos: Discovery of phosphoenolpyruvate phosphomutase which catalyzes the formation of phosphonopyruvate from phosphoenolpyruvate. *J. Antibiot. 42*, 491–494.
12. Seidel, H. M., Freeman, S., Seto, H., and Knowles, J. R. (1988) Phosphonate biosynthesis: Isolation of the enzyme responsible for the formation of a carbon-phosphorus bond. *Nature 335*, 457–458.
13. Kim, J., and Dunaway-Mariano, D. (1996) Phosphoenolpyruvate mutase catalysis of phosphoryl transfer in phosphoenolpyruvate: Kinetics and mechanism of phosphorus-carbon bond formation. *Biochemistry 35*, 4628–4635.
14. Liu, S., Lu, Z., Jia, Y., Dunaway-Mariano, D., and Herzberg, O. (2002) Dissociative phosphoryl transfer in PEP mutase catalysis: Structure of the enzyme/sulfopyruvate complex and kinetic properties of mutants. *Biochemistry 41*, 10270–10276.
15. Nakashita, H., Watanabe, K., Hara, O., Hidaka, T., and Seto, H. (1997) Studies on the biosynthesis of bialaphos. Biochemical mechanism of C-P bond formation: Discovery of phosphonopyruvate decarboxylase which catalyzes the formation of phosphonoacetaldehyde from phosphonopyruvate. *J. Antibiot. 50*, 212–219.
16. Woodyer, R. D., Li, G., Zhao, H., and van der Donk, W. A. (2007) New insight into the mechanism of methyl transfer during the biosynthesis of fosfomycin. *Chem. Commun.*, 359–361.
17. Liu, P., Murakami, K., Seki, T., He, X., Yeung, S. M., Kuzuyama, T., Seto, H., and Liu, H.-w. (2001) Protein purification and function assignment of the epoxidase catalyzing the formation of fosfomycin. *J. Am. Chem. Soc. 123*, 4619–4620.
18. Liu, P., Liu, A., Yan, F., Wolfe, M. D., Lipscomb, J. D., and Liu, H.-w. (2003) Biochemical and spectroscopic studies on (S)-2-hydroxypropylphosphonic acid epoxidase: A novel mononuclear non-heme iron enzyme. *Biochemistry 42*, 11577–11586.
19. Sono, M., Roach, M. P., Coulter, E. D., and Dawson, J. H. (1996) Heme-Containing Oxygenases. *Chem. Rev. 96*, 2841–2888.
20. Ortiz de Montellano, P. R. (1995) *Cytochrome P450: Structure, Mechanism, and Biochemistry*, 2nd ed., Plenum, New York.
21. Lange, S. J., and Que, L., Jr. (1998) Oxygen activating nonheme iron enzymes. *Curr. Opin. Chem. Biol. 2*, 159–172.
22. Kuzuyama, T., Seki, T., Kobayashi, S., Hidaka, T., and Seto, H. (1999) Cloning and expression in *Escherichia coli* of 2-hydroxypropylphosphonic acid epoxidase from the fosfomycin-producing organism, *Pseudomonas syringae* PB-5123. *Biosci., Biotechnol., Biochem. 63*, 2222–2224.
23. Bradford, M. M. (1976) A rapid and sensitive method for the quantitation of microgram quantities of protein utilizing the principle of protein-dye binding. *Anal. Biochem. 72*, 248–254.
24. Hammerschmidt, F. (1991) Labelled representatives of a possible intermediate of fosfomycin biosynthesis in *Streptomyces fradiae*: Preparation of (R,S)-(2-hydroxypropyl)-, (R,S)-, (R)- and (S)-(2-hydroxy-[1,1-$^2H_2$]propyl)- and (R,S)-(2-[^{18}O]hydroxypropyl)phosphonic acid. *Monatsh. Chem. 122*, 389–398.
25. Woschek, A., Wuggenig, F., Peti, W., and Hammerschmidt, F. (2002) On the transformation of (S)-2-hydroxypropylphosphonic acid into fosfomycin in *Streptomyces fradiae*: A unique method of epoxide ring formation. *ChemBioChem 3*, 829–835.
26. Sambrook, J., Fritsch, E. F., and Maniatis, T. (1989) *Molecular Cloning: A Laboratory Manual*, Cold Spring Harbor Laboratory Press, Plainview, NY.
27. Andrews, P. (1964) Estimation of the molecular weights of proteins by Sephadex gel-filtration. *Biochem. J. 91*, 222–233.
28. Fish, W. W. (1988) Rapid colorimetric micromethod for the quantitation of complexed iron in biological smaples. *Methods Enzymol. 158*, 357–364.
29. Paz, M. A., Fluckiger, R., Boak, A., Kagan, H. M., and Gallop, P. M. (1991) Specific detection of quinoproteins by redox-cycling staining. *J. Biol. Chem. 266*, 689–692.
30. Liu, P., Mehn, M. P., Yan, F., Zhao, Z., Que, L., Jr., and Liu, H.-w. (2004) Oxygenase activity in the self-hydroxylation of (S)-2-hydroxypropylphosphonic acid epoxidase involved in fosfomycin biosynthesis. *J. Am. Chem. Soc. 126*, 10306–10312.
31. Yan, F., Munos, J. W., Liu, P., and Liu, H.-w. (2006) Biosynthesis of fosfomycin, re-examination and re-confirmation of a unique Fe(II)- and NAD(P)H-dependent epoxidation reaction. *Biochemistry 45*, 11473–11481.
32. Frisch, M. J., Trucks, G. W., Schlegel, H. B., Scuseria, G. E., Robb, M. A., Cheeseman, J. R., Zakrzewski, V. G., Montgomery, J. A., Jr., Stratmann, R. E., Burant, J. C., Dapprich, S., Millam, J. M., Daniels, A. D., Kudin, K. N., Strain, M. C., Farkas, O., Tomasi, J., Barone, V., Cossi, M., Cammi, R., Mennucci, B., Pomelli, C., Adamo, C., Clifford, S., Ochterski, J., Petersson, G. A., Ayala, P. Y., Cui, Q., Morokuma, K., Malick, D. K., Rabuck, A. D., Raghavachari, K., Foresman, J. B., Cioslowski, J., Ortiz, J. V., Baboul, A. G., Stefanov, B. B., Liu, G., Liashenko, A., Piskorz, P., Komaromi, I., Gomperts, R., Martin, R. L., Fox, D. J., Keith,

T., Al-Laham, M. A., Peng, C. Y., Nanayakkara, A., Gonzalez, C., Challacombe, M., Gill, P. M. W., Johnson, B., Chen, W., Wong, M. W., Andres, J. L., Head-Gordon, M., Replogle, E. S., and Pople, J. A. (1998) *Gaussian98*, Gaussian, Inc., Pittsburgh, PA.

33. Higgins, L. J., Yan, F., Liu, P., Liu, H.-w., and Drennan, C. L. (2005) Structural insight into antibiotic fosfomycin biosynthesis by a mononuclear iron enzyme. *Nature 437*, 838–844.
34. Andersson, M. P., and Uvdal, P. (2005) New scale factors for harmonic vibrational frequencies using the B3LYP density functional method with the triple-ζ basis set 6-311+G(d,p). *J. Phys. Chem. A 109*, 2937–2941.
35. Neese, F., Zumft, W. G., Antholine, W. E., and Kroneck, P. M. H. (1996) The Purple Mixed-Valence CuA Center in Nitrous-oxide Reductase: EPR of the Copper-63-, Copper-65-, and Both Copper-65- and [^{15}N]Histidine-Enriched Enzyme and a Molecular Orbital Interpretation. *J. Am. Chem. Soc. 118*, 8692–8699.
36. Yan, F., Li, T., Lipscomb, J. D., Liu, A., and Liu, H.-w. (2005) Site-directed mutagenesis and spectroscopic studies of the iron-binding site of (S)-2-hydroxypropylphosphonic acid epoxidase. *Arch. Biochem. Biophys. 442*, 82–91.
37. Zhao, Z., Liu, P., Murakami, K., Kuzuyama, T., Seto, H., and Liu, H.-w. (2002) Mechanistic studies of HPP epoxidase: Configuration of the substrate governs its enzymatic fate. *Angew. Chem., Int. Ed. 41*, 4529–4532.
38. Hammerschmidt, F. (1991) Biosynthesis of natural products with a phosphorus-carbon bond. Part 8. On the origin of the oxirane oxygen atom of fosformycin in *Streptomyces fradiae*. *J. Chem. Soc., Perkin Trans. 8*, 1993–1996.
39. Yan, F., Moon, S. J., Liu, P., Zhao, Z., Lipscomb, J. D., Liu, A., and Liu, H.-w. (2007) Determination of the substrate binding mode to the active site iron of (S)-2-hydroxypropylphosphonic acid epoxidase using ^{17}O-enriched substrates and substrate analogues. *Biochemistry 46*, 12628–12638.
40. Solomon, E. I., Brunold, T. C., Davis, M. I., Kemsley, J. N., Lee, S. K., Lehnert, N., Neese, F., Skulan, A. J., Yang, Y. S., and Zhou, J. (2000) Geometric and electronic structure/function correlations in non-heme iron enzymes. *Chem. Rev. 100*, 235–350.
41. Costas, M., Mehn, M. P., Jensen, M. P., and Que, L., Jr. (2004) Dioxygen activation at mononuclear nonheme iron active sites: Enzymes, models, and intermediates. *Chem. Rev. 104*, 939–986.
42. Baldwin, J. E., and Bradley, M. (1990) Isopenicillin N synthase: Mechanistic studies. *Chem. Rev. 90*, 1079–1088.
43. Brown, C. D., Neidig, M. L., Neibergall, M. B., Lipscomb, J. D., and Solomon, E. I. (2007) VTVH-MCD and DFT studies of thiolate bonding to $[FeNO]_7$/$[FeO_2]_8$ complexes of isopenicillin N synthase: Substrate determination of oxidase versus oxygenase activity in nonheme Fe enzymes. *J. Am. Chem. Soc. 129*, 7427–7438.
44. Price, J. C., Barr, E. W., Tirupati, B., Bollinger, J. M., Jr., and Krebs, C. (2003) The first direct characterization of a high-valent iron intermediate in the reaction of an α-ketoglutarate-dependent dioxygenase: A high-spin FeIV complex in taurine/α-ketoglutarate dioxygenase (TauD) from *Escherichia coli*. *Biochemistry 42*, 7497–7508.
45. Eser, B. E., Barr, E. W., Frantom, P. A., Saleh, L., Bollinger, J. M., Jr., Krebs, C., and Fitzpatrick, P. F. (2007) Direct Spectroscopic Evidence for a High-Spin Fe(IV) Intermediate in Tyrosine Hydroxylase. *J. Am. Chem. Soc. 129*, 11334–11335.
46. Koehntop, K. D., Emerson, J. P., and Que, L., Jr. (2005) The 2-His-1-carboxylate facial triad: A versatile platform for dioxygen activation by mononuclear non-heme iron(II) enzymes. *J. Biol. Inorg. Chem. 10*, 87–93.
47. Hashimoto, T., Matsuda, J., and Yamada, Y. (1993) Two-step epoxidation of hyoscyamine to scopolamine is catalyzed by bifunctional hyoscyamine 6β-hydroxylase. *FEBS Lett. 329*, 35–39.
48. Busby, R. W., and Townsend, C. A. (1996) A single monomeric iron center in clavaminate synthase catalyzes three nonsuccessive oxidative transformations. *Bioorg. Med. Chem. 4*, 1059–1064.

BI800877V